Single Wall Carbon Nanotube/Polyethylene Nanocomposites: Nucleating and Templating Polyethylene Crystallites

Reto Haggenmueller, John E. Fischer, and Karen I. Winey*

Department of Materials Science and Engineering, University of Pennsylvania, Philadelphia, Pennsylvania 19104-6272

Received December 28, 2005; Revised Manuscript Received February 1, 2006

ABSTRACT: The crystallization kinetics and resulting morphology of polyethylene (PE) in the presence of single wall carbon nanotubes (SWNT) are investigated in isotropic and aligned composites. A hot coagulation method was developed to incorporate SWNT loadings as high as 30 wt % with uniform distribution. Thermal analysis interpreted using the Avrami equation showed that the nanotubes provide nucleation sites to PE and accelerate the PE crystal growth rate while reducing the crystal dimensionality from spherulitic to disk-shaped. Nucleating on SWNT bundles significantly increases the shish density during melt fiber spinning, so that the PE microstructure is shish kebab with straight (not twisted) lamellae in 1 wt % SWNT−HDPE composite fibers. By comparing the orientations of SWNT and PE produced by various processing conditions, we show that SWNT bundles template the growth of PE crystals by imposing a growth direction perpendicular to the SWNT. This provides a new route toward controlling the SWNT−polymer interface and thereby the physical properties of nanocomposites.

Introduction

Carbon nanotubes are promising fillers for polymer composites due to their extraordinary mechanical, electrical, and thermal properties. However, numerous investigations demonstrate only modest improvements in mechanical and thermal properties relative to the polymer matrix, indicating that the effectiveness of SWNT relies not only on the intrinsic properties of SWNT but also on composite characteristics such as nanotube dispersion and alignment and polymer matrix structure in the presence of nanotubes. Furthermore, the interface between SWNT and matrix is a key parameter for the final nanocomposite properties.

The polymer matrix structure and the interface are especially strongly influenced by SWNT in semicrystalline polymer composites because the nanotubes have the potential to nucleate the polymer crystallization.[1−4] Bhattacharyya et al. showed that only 0.8 wt % SWNT in polypropylene nucleate crystallization, which results in substantially reduced spherulite size and crystallization half-times.[1] Grady et al. demonstrated similar effects with 0.6 wt % octadecylamine functionalized SWNT in polypropylene and also found a change of the Avrami exponent.[2] The presence of as little as 0.1 wt % SWNT in poly(vinyl alcohol) distinctively nucleated the PVA crystallization as shown by Probst et al.[3]

The structure of the nucleated crystalline polymer layer on SWNT is of particular interest. Transcrystallinity, where nucleation occurs at a fibrous filler and oriented crystallization progresses radially from the fibers surface, occurs in traditional semicrystalline polymer composites with fibrous fillers like UHMWPE, carbon, or glass fibers.[5−7] For example, highly oriented crystalline layers on the filler surface exist in polyethylene/polyethylene composites in which transcrystalline growth starts epitaxially with the *c*-axis aligned in the fiber axis, and the lamellae twist as the crystallites grow outward from the fiber.[5] Transcrystallinity and twisting lamella are also observed in aramid fiber−polypropylene composites where a 90° twist of the parent lamellae occurs within ∼25 μm from the fiber, followed by untwisted lamellae growth.[6] Bogoeva-Gaceva et al. showed that coatings on glass fibers improve mechanical properties by promoting nucleation and transcrystallinity of polypropylene.[7]

While transcrystallinity has not been detected in nanotube/polymer composites, there are indications that SWNT could nucleate transcrystalline layers. Wei et al. used molecular dynamics simulations to show that amorphous polyethylene (PE) form an adsorption layer on isolated SWNT in which the PE chains preferably align parallel to the nanotube axis.[8] Furthermore, Li et al. crystallized PE in a dilute solution along with SWNT or MWNT and found PE crystallites perpendicular to the nanotube axis.[9] Here we investigate the melt crystallization kinetics and structure of PE in the presence of small SWNT bundles and demonstrate that the polyethylene layer on the SWNT is indeed transcrystalline.

Experimental Section

Materials and Composite Fabrication. The matrix polymers were low-density and high-density polyethylene (LDPE MW ∼ 35 000 g/mol and HDPE ∼ 50 000 g/mol, supplied by Aldrich) with crystallinities of 33% and 78%, respectively. SWNT for the nanocomposites were synthesized by the laser ablation method (supplied by NASA Johnson Space Center) and purified with a soft bake at 300 °C for 6 h followed by sonication in 12 M HCl at 80 °C for 35 min and washing thereafter, resulting in a catalyst content below 5 wt % as determined by thermal gravimetric analysis.

The hot-coagulation method, an adaptation of the previously described coagulation method,[10] produced the SWNT−polyethylene composites. Specifically, HDPE and LDPE were dissolved at 115 and 85 °C, respectively, in 1,2-dichlorobenzene (DCB) at a concentration of 20 mg/mL. SWNT were suspended in DCB at 0.2 mg/mL using an ultrasonic bath sonicator for 48 h. Then the sonication bath temperature was increased to 97 °C, and the hot PE solution was added to the nanotube suspension. After further sonication for 5 min the mixture was cooled below ∼70 °C to crystallize the PE. The resulting SWNT−PE suspension was visually homogeneously light gray and remained stable for several hours. Composites obtained after filtration were dark-gray and the supernatant was clear, indicating that the nanotubes were incorporated in the PE matrix. While drying under vacuum at 150 °C the composites densified and turned black. Composites were prepared with 1, 2,

* Corresponding author. E-mail: winey@seas.upenn.edu.

10.1021/ma0527698 CCC: $33.50
Published on Web 03/10/2006

Table 1. Melt Fiber Spinning Processing Parameters for HDPE and SWNT−HDPE Composites at Various SWNT Loadings and Wind-Up Speeds[a]

	wind-up speed [m/min]											
	0	10	20	30	40	60	80	100	120	125	140	160
HDPE			2	1	2	1, 2	2	2	2	1	2	1, 2
1 wt % NT−HDPE	2		2		2	2	2	2	*f*			
2 wt % NT−HDPE	2	2	2	*f*								
5 wt % NT−HDPE	2	*f*										

[a] The listed values (1 or 2) indicate the extrusion speeds in mm/min. Blank fields indicate conditions that were not attempted, and *f* indicates that melt fiber spinning failed. Rods were extruded without fiber drawing, as indicated by 0 m/min wind-up speed.

5, 10, and 30 wt % SWNT in HDPE and with 1 and 30 wt % SWNT in LDPE.

Processing and Characterization. Dried composites were compression-molded at 110 and 150 °C to produce LDPE and HDPE composites, respectively, using a window mold (10 mm × 5 mm × 1 mm). Composite fibers with aligned SWNT and HDPE chains were melt-spun using a DACA SpinLine consisting of a single spinneret hole (500 μm) attached to a heated barrel with a piston extruder. The extruded fiber was air-cooled and drawn under tension with a variable-speed winder. Neat HDPE and 1 and 2 wt % SWNT−HDPE composites were spun at 160 °C using different extrusion and wind-up speeds. Melt-spun fibers are designated as *X* wt % NT-HDPE-*Y*-*Z*, where *X* is the SWNT loading, *Y* is the extrusion speed in mm/min, and *Z* is the wind-up speed in m/min (Table 1). The piston diameter is 10 mm.

The size distribution of the nanotube bundles in DCB suspensions prior to making the composites was measured using tapping mode atomic force microscopy (AFM, Nanoscope III, Digital Instruments Inc.).[11] A silicon wafer, which was precleaned by ∼1 min sonication in acetone, was dipped into a ∼0.2 mg/mL SWNT−DCB suspension for ∼2 s to collect enough nanotube bundles on the wafer for AFM analysis. Few nanotube bundles overlapped which allowed for accurate length and height measurements, and 270−400 bundles were thus characterized.

Transmission light microscopy on hot-pressed films (∼100 μm thick) was used to globally evaluate the distribution of SWNT within the composites. A more detailed characterization of the local SWNT distribution was obtained from SEM studies. Samples were broken after cooling in liquid nitrogen and coated with Pt/Au for fracture surface analysis in a SEM (JEOL 6300FV). The PE spherulite structure in neat HDPE and SWNT composites was imaged by cross-polarized optical microscopy on thin films obtained by crystallizing from a ∼115 °C DCB solution on a hot glass slide.

Thermal analysis was performed using a Perkin-Elmer differential scanning calorimeter (DSC 7). For isothermal crystallization, samples were melted at 160 °C for 10 min to erase the thermal history, quenched at 300°/min to the desired crystallization temperature, T_c, and held at T_c until the crystallization was complete. The relative crystallinity as a function of time was obtained by integrating the heat flow vs time data. The quench rate is sufficiently fast to measure the rapid crystallization of HDPE and composites with 1 and 10 wt % SWNT, but crystallization in 30 wt % SWNT composites could not be assessed, as it was too rapid. Nonisothermal crystallization experiments involve melting at 160 °C for 10 min followed by cooling at 10 °C/min.

Wide-angle X-ray scattering (WAXS) was used to assess the orientation of the PE crystallites in the hot-pressed samples and melt-spun fibers. Measurements were performed in transmission on the University of Pennsylvania's multiple-angle X-ray scattering (MAXS) apparatus equipped with a 2-D wire detector.[12] Two-dimensional scattering patterns were integrated along the radial direction, q, across the (110) and (200) Bragg reflections of PE at $2\theta = 21.6°$ and 24° ($q = 1.52$ and 1.69 Å^{-1}) to give scattered intensity as a function of the azimuthal angle, χ.

The degrees of SWNT alignment in the hot-pressed PE composites were determined directly from azimuthal widths of radial q integrations ($q = 0.015-0.075$ Å^{-1}) of small-angle X-ray scattering (SAXS) patterns. In hot-pressed PE composites the low q intensity is dominated by form factor scattering from SWNT;[13] in fact, the low angle scattering in the 10 wt % composite no longer exhibits a maximum corresponding to PE crystallites but rather exhibits smooth decrease in scattering intensity in this angular range. The same could not be done for the melt-spun composite fibers because scattering from oriented PE crystals dominates in this q range. Consequently, the SWNT orientation in composite fibers was evaluated from polarized Raman spectroscopy (Renishaw micro-Raman spectrometer in VV polarization geometry (1 μm beam spot) and 514.5 nm excitation). Three positions along the fiber were measured at $\psi = 0°$ and 90°, where ψ is the angle between the fiber axis and the polarization vector of the incident light. The Raman intensity ratio ($I_{0°}/I_{90°}$) is used to estimate the fwhm of a Lorentzian distribution of SWNT axes with respect to the fiber axis.[14,15] This method assumes that the entire sample volume contains aligned SWNT (i.e., no unaligned fraction), which is reasonable for melt-spun composite fibers with modest SWNT loadings.

Results and Discussion

SWNT Characterization and Dispersion in Composites. Composite properties depend on the aspect ratio of the fillers. Recent models which assume identical, isolated, and isotropic nanotubes predict that increasing the aspect ratio improves the electrical and thermal conductivity.[16−18] Experimentally, nanotubes in polymer composites exist predominately in small-diameter bundles at the concentrations considered here. To access the aspect ratios of these bundles, AFM images were collected from nanotube bundles in DCB suspensions prior to hot coagulation (Figure 1a). The average length and diameter are 445 and 3 nm, respectively, and the average correlated aspect ratio (Figure 1b), calculated from length and height measured for each nanotube bundle, is 212. A bundle diameter of 3 nm corresponds to ∼4−7 nanotubes. Upon cooling the mixture of PE and SWNT bundles in DCB, PE crystallizes and rapidly entraps the SWNT bundles, thereby preventing the slower process of SWNT agglomeration. Thus, the SWNT bundle sizes determined in DCB are indicative of the SWNT bundles in PE.

Our hot-coagulation method produces composites with overall homogeneous SWNT distribution on the 10 μm scale as probed by optical microscopy (Figure 2a). A few particles are detected that originate from SWNT agglomerates that persist while sonicating the DCB suspensions. SEM images of fracture surfaces clearly show bundles that are homogeneously distributed in the polymer matrix, forming continuous networks, especially in composites with high nanotube loading (Figure 2c). Composites made from either HDPE or LDPE show well-dispersed SWNT bundles, as evaluated by optical microscopy and SEM.

Our hot-coagulation method efficiently prepares SWNT−polymer composites with high nanotube loadings and good SWNT homogeneity by rapidly incorporating the entire quantity of SWNT into the polymer matrix in one step. By comparison, our earlier melt-blending method in which SWNT was added in small increments to maintain good dispersion results in a slower fabrication method.[15] In-situ polymerization methods are also one-step processes, but the nanotubes can interfere with

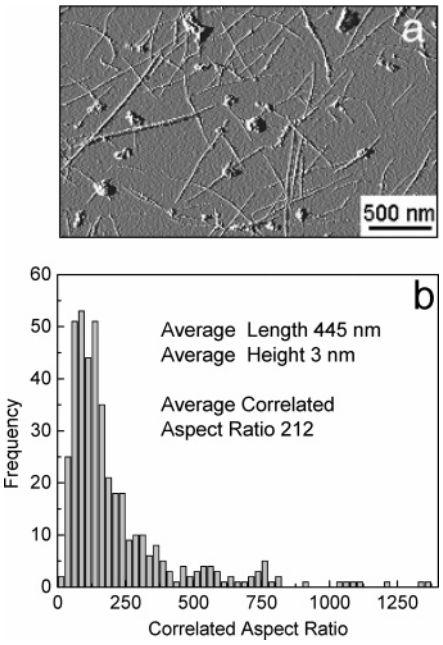

Figure 1. AFM image of NASA tubes deposited from DCB, 0.2 mg/mL, after 35 h sonication (a) and the corresponding aspect ratio distribution (b).

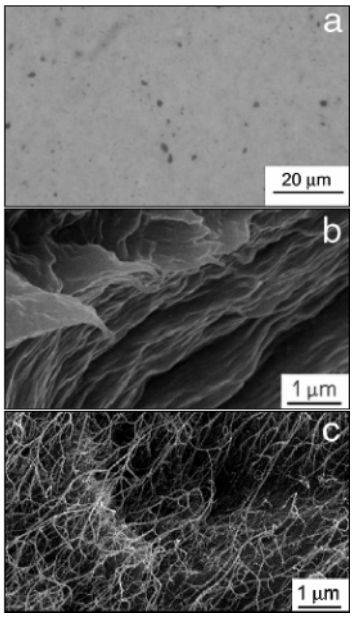

Figure 2. Transmission optical micrograph of a hot-pressed 1 wt % NT−HDPE composite film (a) and SEM images of fracture surfaces of LDPE (b) and a 30 wt % NT−LDPE composite (c).

the polymerization reaction and reduce the resulting polymer molecular weight as shown for nylon.[19,20] The hot-coagulation method is applicable to any thermoplastic solution exhibiting a miscibility transition upon cooling, while also avoiding the large volume of excess solvent required in our original coagulation method.

PE Crystallinity in Hot-Pressed Samples. The interface between SWNT and a polymer matrix significantly influences the composite properties; e.g., the interfacial thermal resistance is a key factor in the thermal conductivity of heterogeneous systems.[21] The semicrystalline morphology of PE allows for the nanotubes to be in contact with highly ordered crystallites and/or amorphous domains, where the interfacial PE morphology might dramatically impact the composite thermal properties.

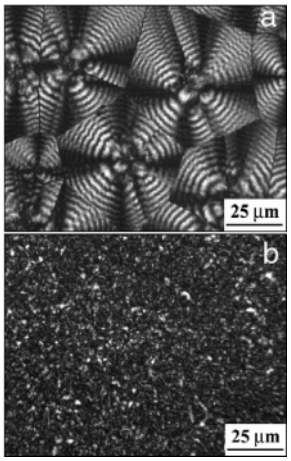

Figure 3. Transmission optical micrographs with crossed polarizers of (a) thin HDPE and (b) 0.25 wt % NT−HDPE films, crystallized on a glass slide from a DCB solution.

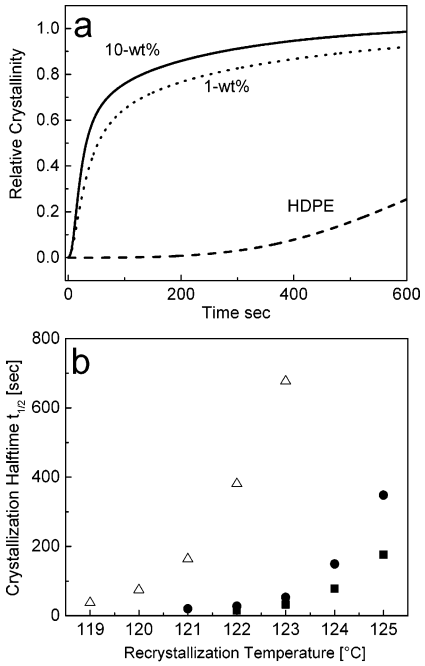

Figure 4. (a) Relative crystallinity at 123 °C obtained by integration of the heat flow as a function of time and (b) half-time of crystallization measured at 50% relative crystallinity vs crystallization temperature for (△) HDPE, (●) 1 wt % NT−HDPE, and (■) 10 wt % NT−HDPE composite. Note that these isothermal crystallization studies continued for times >600 s.

The presence of SWNT dramatically increases the number of nucleation sites and thereby decreases the average crystallite size as detected by polarized optical microscopy (Figure 3). In the absence of SWNT, HDPE forms large spherulites (∼30−50 μm) with twisted lamellae when crystallized from DCB solution. In contrast, the crystal structure in SWNT−HDPE composites with ∼0.25 wt % nanotube loading consists of smaller crystallites (∼1−5 μm). Given the additional nucleation sites in SWNT−HDPE composites, the rate of isothermal crystallization is dramatically faster; Figure 4a plots the relative crystallinity vs time at 123 °C. The half time of crystallization ($t_{1/2}$) is the time required to accomplish 50% of the crystallization under isothermal conditions (Figure 4b). The addition of 1 wt % SWNT reduces $t_{1/2}$ to ∼7% of the HDPE $t_{1/2}$ at 122 °C; the reduction in $t_{1/2}$ is even greater at 123 °C. Increasing the SWNT loading from 1 to 10 wt % provides only a modest additional decrease in $t_{1/2}$, suggesting that enough

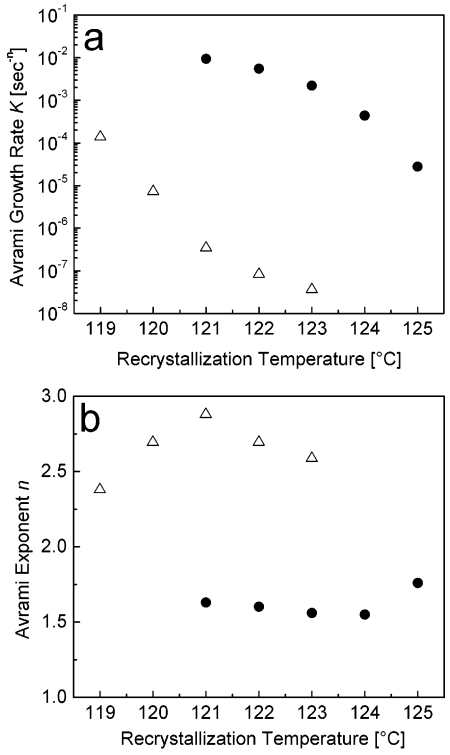

Figure 5. (a) Kinetic growth constant K of Avrami equation. (b) Avrami exponent n for (△) HDPE and (●) 1 wt % NT−HDPE. The Avrami equation was fit to relative crystallinity data (Figure 4) from 5 to 30%.

nanotubes are present at 1 wt % to provide sufficient surface area so that crystal growth, rather than crystallite nucleation, becomes rate limiting. A similar, though less dramatic, trend was observed by Grady et al.[2] in nanocomposites of polypropylene and SWNT functionalized with octadecylamine; the $t_{1/2}$ of polypropylene in those composites was reduced by a factor of ∼2 at both 0.6 and 1.8 wt % SWNT loading.

Crystallization kinetics were modeled with the Avrami equation for isothermal crystallization:

$$X_r(t) = 1 - \exp(-Kt^n) \quad (1)$$

where X_r is the relative crystallinity, n is the Avrami exponent, K is the kinetic rate constant, and t is the crystallization time. (In Figure 4a the short time data appear highly compressed, but log t vs log(−ln(1 − X_r)) plots capture the induction period and exhibit linear regimes to allow the Avrami analysis.) Values of n and K are determined from HDPE (T_c = 119−123 °C) and 1 wt % NT−HDPE (T_c = 121−125 °C) using data from X_r = 5−30%; the faster crystallization in 10 wt % NT−HDPE composites made the analysis unreliable. The Avrami growth rates (K) are much faster for the 1 wt % composite than for HDPE (Figure 5a). Both data sets approach a maximum in K with decreasing temperature, which is consistent with limited enthalpy gain at higher temperatures and limited diffusion at lower temperatures. The Avrami exponent (n) for HDPE is ∼2.5−3, indicating spherulitic growth,[22] while n for the 1 wt % composite is ∼1.6 (Figure 5b). An exponent between 1 and 2 corresponds to disk-shaped growth, indicating a change in the HDPE microstructure and crystalline growth in the presence of SWNT bundles. In contrast, Grady et al. found an increase of the Avrami exponent from ∼2.2 for polypropylene to ∼2.8 for 0.6% nanotubes,[2] which could not be assigned to a specific crystalline geometry.

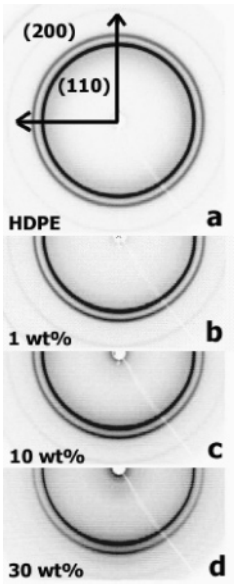

Figure 6. Wide-angle X-ray diffraction patterns of hot-pressed (a) HDPE, (b) 1 wt %, (c) 10 wt %, and (d) 30 wt % NT−HDPE composites. The arrows (a) indicate the meridional (vertical) and equatorial (horizontal) direction. Pressing direction is along the meridian. Diffraction from (110) and (200) are at 2θ = 21.6° and 24° (q = 1.52 and 1.69 Å^{-1}), respectively.

The nonisothermal crystallization experiments also demonstrate the ability of SWNT to accelerate the crystallization kinetics of PE. Upon cooling from $T > T_m$ at 10 °C/min, the observed crystallization temperatures for the composites are 5 °C above that of the neat HDPE, signifying that SWNT nucleate the PE crystallization. Note that all the SWNT−HDPE composites (1−30 wt %) exhibit the same 5 °C increase relative to HDPE, indicating that 1 wt % SWNT provides sufficient nucleation sites so that nucleation is no longer rate limiting. Independent of the crystallization process, the melting temperatures are constant, and the overall crystallinities are constant at 78% and 33% for LDPE and HDPE, respectively.

In summary, SWNT bundles act as nucleation sites when PE crystallizes, indicating that the initial crystallites of PE are in contact with the nanotubes. Furthermore, Avrami analysis shows that nucleation on the highly anisotropic SWNT bundles changes the microstructure of the PE crystallites from spherulites to disks.

Morphology of Nominally Isotropic Composites. The (110) and (200) reflections (2θ = 21.6° and 24°, respectively) indicate that hot-pressed PE is indeed isotropic (Figure 6a). In contrast, hot-pressed SWNT−PE composites are slightly anisotropic as shown by an increased intensity on the meridian (pressing direction), with underlying isotropic scattering (Figure 6b−d). This anisotropic scattering from the composite indicates weakly preferred orientation of the PE chain axis (c-axis of orthorhombic lattice) perpendicular to the pressing direction. The anisotropy becomes more pronounced (but still weak) as the SWNT loading increases in both LDPE and HDPE. The q-integration of the (110) reflection after subtracting the isotropic scattering was plotted as a function of χ and fitted with a Gaussian distribution function. The resulting full width at half-maximum (fwhm) quantitatively describes the degree of PE alignment in the hot-pressed composites: fwhms are ∼65° and 55° for 10 and 30 wt % SWNT composites. The intensity ratio at meridional and equatorial angles $I_{90°}/I_{0°}$ of the (110) reflection increases from 1.6 for 1 wt % to 2.5 for 30 wt % NT−HDPE composites, which indicates that there still is a significant unaligned portion of HDPE at 30 wt % SWNT. The orientation

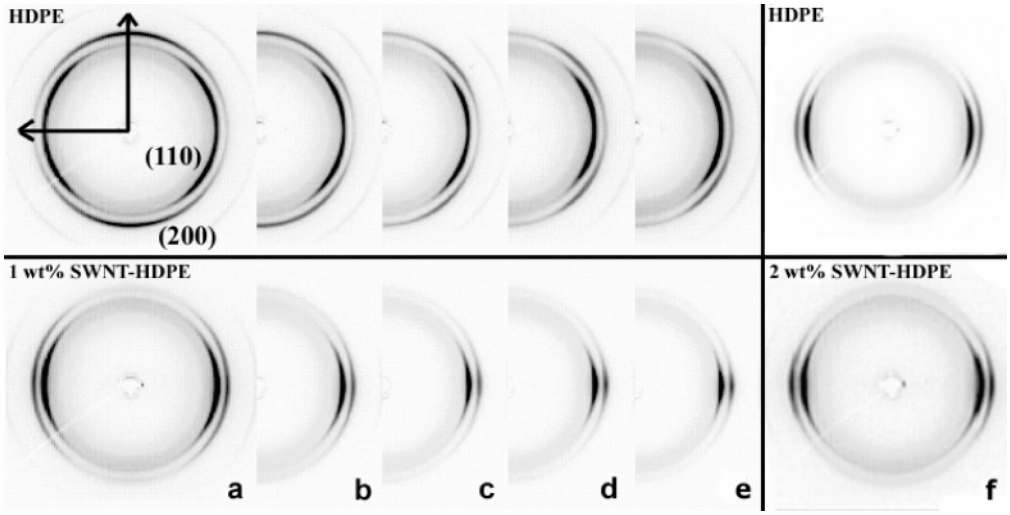

Figure 7. Wide-angle X-ray diffraction patterns of HDPE (top row) and SWNT composites (bottom row) fibers. Spinning parameters are 2 mm/min extrusion speed and 20, 40, 60, 80, and 100 m/min wind-up speed for rows (a)−(e). Top row (f) is the result for HDPE at 160 m/min wind-up speed (HDPE-1-160); bottom row (f) is the result of higher SWNT loading, 2 wt % NT-HDPE-2-20. Fiber direction is meridian. The arrows in top row (a) indicate the meridional (vertical) and equatorial (horizontal) direction. Diffraction from (110) and (200) are at $2\theta = 21.6°$ and 24° ($q = 1.52$ and 1.69 Å^{-1}), respectively.

in the plane perpendicular to the pressing direction is isotropic (data not shown). HDPE and LDPE composites show similar trends in PE orientation at a given nanotube loading.

Preferred orientation of the SWNT in these hot-pressed composites was evaluated by SAXS. The SAXS patterns from the nanotubes are oblong, indicating a slightly preferred orientation of SWNT perpendicular to the pressing direction.[12] This anisotropy of SWNT scattering is more pronounced at higher SWNT loadings. A *q*-integration of the SWNT scattering was fit with a Gaussian function, the fwhm of which serves to quantify the SWNT anisotropy. For example, the 30 wt % NT−HDPE composite exhibits a fwhm of ∼60°. Thus, the orientations of both the PE crystallites and the SWNT are similar, indicating that in addition to nucleating the crystallization process the presence of SWNT bundles impacts the orientation of the crystal growth. The orientation of SWNT templates the PE orientation, and this observation become more evident in the highly aligned composites discussed below.

Morphology of Highly Oriented Composites. Preferred orientation of SWNT in composite fibers was estimated from polarized Raman spectroscopy intensity ratios, as described above. A Lorentzian distribution of SWNT axes relative to the fiber axis is assumed, and a fwhm based on the Raman ratio semiquantitatively describes the SWNT alignment.[14,23] Systematic variations with processing conditions are more significant than absolute values. The nanotubes in the 1 and 2 wt % SWNT−HDPE composite fibers are well aligned in the fiber direction at low wind-up speeds (20 m/min) with fwhm of ∼8° and 11°, respectively. Higher wind-up speeds were achieved using the 1 wt % composite (Table 1) and produce a modest increase in alignment (fwhm = ∼4°). Increasing elongational flow during melt fiber spinning by increasing wind-up speeds improves the SWNT alignment, especially at low SWNT loadings where there are fewer nanotube−nanotube constraints to limit orientation. Nanotubes in the extruded rods (0 m/min wind-up speed) have only a slightly preferred orientation in the direction of the fiber axis (∼95° for 1 and 2 wt % and ∼ 64° for 5 wt % NT−HDPE composites), as expected for smaller extensional forces.

The WAXS patterns of HDPE fibers show (110) and (200) diffraction peaks at distinct azimuthal positions that depend on the spinning parameters of extrusion speed and wind-up speed. HDPE fibers that were extruded at 2 mm/min show a (110) four-point pattern (two (110) intensity maxima of either side of the equator) at all wind-up speeds (Figure 7a−e, top). The (110) peaks move toward the equator as the wind-up speed increases. HDPE fibers that were extruded at 1 mm/min show a (110) four-point pattern at low wind-up speeds (30 and 60 m/min) and a (110) two-point pattern ((110) peaks centered on the equator) at high wind-up speeds (125 and 160 m/min) (see Figure 7f, top). The (200) diffraction peaks of these HDPE fibers are centered on the meridian for low wind-up speeds (Figure 7a, top). The (200) diffraction peaks are positioned between meridian and equator at modest wind-up speeds and centered at the equator at high wind-up speeds (Figure 7f, top).

The positions of the HDPE (110) and (200) WAXS diffraction peaks are characteristic of the shish-kebab morphology, which was first described by Keller and Machin[24] for melt-spun polyethylene fibers. The extensional flow of the melt spinning process extends and orients PE chains along the flow direction, such that these PE chains crystallize in fibrillar form. These fibrillar structures are the shishes of the model. More relaxed PE chains between the shishes crystallize in lamellar form and grow perpendicular to the shish direction, called kebabs. At a low shish density, the kebabs twist as they radially grow, similar to quiescent growth in PE spherulites. At high shish density, resulting from increased extensional forces, the crowded kebabs grow outward from the shishes without twisting. Schematic WAXS patterns are shown for twisted and non-twisted shish-kebab microstructures in Figure 8.[25,26] Comparing Figure 7 (top) and Figure 8, we conclude that the shish-kebab morphology in HDPE transitions from twisted to straight lamellae as the extensional flow increases.

In contrast, WAXS patterns of the 1 and 2 wt % SWNT−HDPE composite fibers have (110) and (200) peaks at the equator for all extrusion and wind-up speeds (Figure 7, bottom row). In the presence of SWNT bundles the shish-kebab PE morphologies have only straight lamellae due to the higher density of shishes. Increasing extensional flow in the melt-spun fibers (higher extrusion and wind-up speeds) improves the SWNT alignment, and these aligned SWNT effectively nucleate PE crystallization. Apparently, the nucleation and crystallization of PE predominately occur at the aligned SWNT bundles rather than at extended PE shishes. These additional nucleation sites

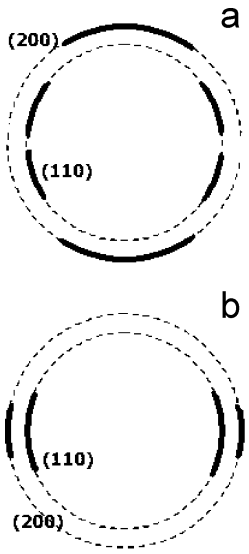

Figure 8. Schematic WAXS patterns for shish kebabs with (a) twisted and (b) nontwisted kebabs indicative of low and high shish densities, respectively. Shish-kebab direction is meridional.

relative to neat HDPE fibers increase the shish density and prevent twisting during lamellae growth. Again, we note that the SWNT bundles both nucleate and template the PE crystallization.

Extruded neat HDPE rods (zero wind-up speed) have isotropic PE. Rods from the 1, 2, and 5 wt % SWNT−HDPE composites show broad single (110) and (200) peaks, which are centered at the equator, indicating modestly aligned shish kebabs with straight kebabs. According to polarized Raman spectroscopy, SWNT in the extruded rods have only a moderately preferred orientation in the direction of the fiber axis. As seen above for composite fibers, the twisting of the lamellae is reduced due to the higher density of nucleation sites provide by the SWNT bundles, and the orientation of the SWNT dictates the PE orientation in the composite rods.

We use the Hermans[27] orientation factor, f_c, to quantify the PE orientation

$$f_c = \frac{3\langle\cos^2\phi_c\rangle - 1}{2} \tag{2}$$

where ϕ_c is the angle between the fiber or rod direction and the *c*-axis of orthorhombic PE crystal corresponding to the chain direction. The term $\langle\cos^2\phi_c\rangle$ is defined as

$$\langle\cos^2\phi_c\rangle = \frac{\int_0^{\pi/2} I(\phi)\cos^2\phi\sin\phi\,\mathrm{d}\phi}{\int_0^{\pi/2} I(\phi)\sin\phi\,\mathrm{d}\phi} \tag{3}$$

where $I(\phi)$ are the diffracted intensity from the planes normal to the *c*-axis. These orientations are normally obtained from (200) and (020) reflections, but because the (020) reflection is missing, we use Wilchinsky's method.[28] Thus, we calculate $\langle\cos^2\phi_c\rangle$ using the (110) and (200) reflections, the angle between the normal of the (110) plane and the *a*-axis (56.6° for PE), and the orthogonality relationship in the orthorhombic crystal structure, $\langle\cos^2\phi_a\rangle + \langle\cos^2\phi_b\rangle + \langle\cos^2\phi_c\rangle = 1$:

$$\langle\cos^2\phi_c\rangle = 1 - 0.565\langle\cos^2\phi_{200}\rangle - 1.435\langle\cos^2\phi_{110}\rangle \tag{4}$$

When $f_c = -0.5$, 0, and 1, the *c*-axis is perpendicular, random, and parallel relative to the fiber direction, respectively. Using these same methods, the orientation factors (f_a and f_b) are calculated between the *a*-axis and *b*-axis relative to the fiber direction.

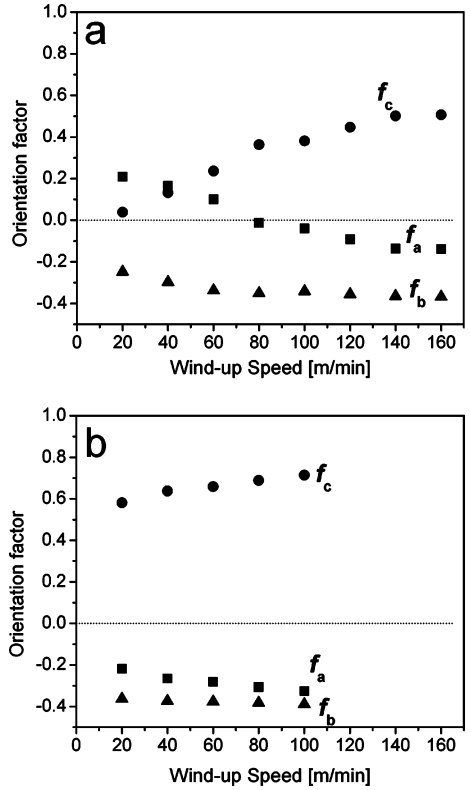

Figure 9. Hermans orientation factors as a function of wind-up speed for (a) HDPE fibers and (b) 1 wt % NT−HDPE composite fibers extruded at 2 mm/min.

The orientation factors for HDPE show the typical change from *b*-axial alignment to *c*-axial alignment, as f_c increases and f_a and f_b decrease with increasing wind-up speed (Figure 9a). These orientation factors are consistent with the shish-kebab morphologies having twisted and straight lamellae at low and high wind-up ratios, respectively. In contrast, the 1 wt % NT−HDPE composite fibers show *c*-axis alignment at all wind-up speeds, indicating shish kebabs with straight lamellae (Figure 9b). Note that at fixed extrusion and wind-up speeds preferred orientation in the composite fibers is more pronounced than in HDPE fibers. For example, at 2 mm/min extrusion speed and 100 m/min wind-up speed, f_c is 0.38 and 0.72 for HDPE and 1 wt % NT−HDPE, respectively. Additional f_c data in Figure 10 for various processing conditions show that increasing SWNT loading can further increase f_c. The orientation of the SWNT bundles in the composite rods and fibers produced by extensional flow improves the orientation of the PE crystallites because SWNT nucleate and template PE crystallization.

The SAXS patterns from all the HDPE fibers show the typical lobes on the meridian attributed to alternating crystalline (kebab) and amorphous regions of the shish-kebab microstructure (Figure 11a).[26] A weak second-order peak is observed on the meridian, indicating regular stacking of lamellar and interlamellar amorphous regions (data not shown). SAXS patterns of SWNT−HDPE composite fibers also show intensity maxima on the meridian, but the shape is a streak, rather than a lobe (Figure 11b). The average distances between the centers of the crystalline parts, namely the long periods, were calculated using the first-order maxima and found to be independent of the wind-up speed. The long period in HDPE fibers is ∼20 nm and

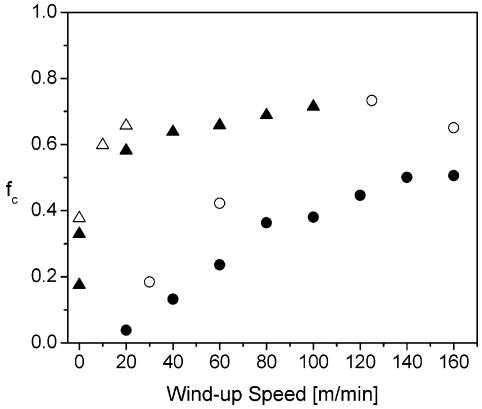

Figure 10. Hermans orientation factor f_c as a function of wind-up speed (*Z*) for (●) HDPE-2-*Z*, (○) HDPE-1-*Z*, (▲) 1 wt % NT−HDPE-2-*Z*, and (△) 2 wt % NT−HDPE-2-*Z*.

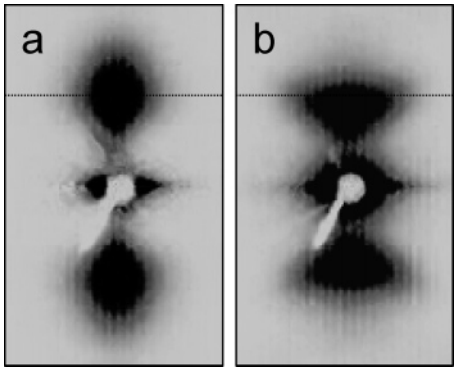

Figure 11. Small-angle X-ray diffraction patterns of (a) HDPE-2-100 and (b) 1 wt % NT−HDPE-2-100 (right). Fiber direction is along the meridian. The horizontal line marks $q = 0.03$ Å^{-1}.

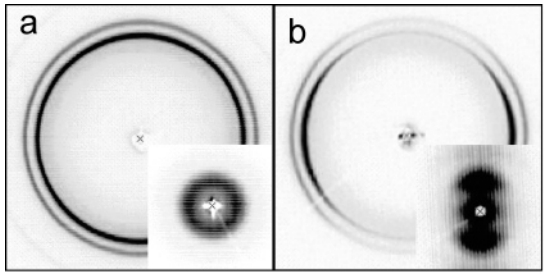

Figure 12. WAXS and SAXS (inset) patterns of (a) HDPE-2-100 and (b) 1 wt % NT−HDPE-2-100 after melting on a glass slide. Fiber axis before melting is along the meridian.

increases slightly to ∼21.5 and ∼23 nm for 1 and 2 wt % NT−HDPE composite fibers, respectively.

Recrystallization of SWNT−HDPE Composite Fibers. During melt fiber spinning of SWNT−HDPE composites the observed PE orientation might arise from a combination of templating on the aligned SWNT bundles and the extensional flow field. We probe the relative importance of these two contributions by recrystallizing SWNT−HDPE composite fibers in the absence of flow. Recrystallized HDPE fibers show isotropic WAXS and SAXS patterns (Figure 12a), demonstrating, as expected, that the PE chains lost their preferred orientation upon melting. WAXS patterns of recrystallized composite fibers have (110) and (200) maxima on the equator, consistent with a shish-kebab morphology (Figure 12b). The f_c of the PE crystallites decreases upon recrystallization of composite fiber, for example from 0.72 to 0.35 in 1 wt % NT−HDPE-2-100 fibers. A lobe pattern persists in SAXS for the recrystallized composite fibers (Figure 12b, inset). Here the SWNT orientation also deteriorates with recrystallization as evidenced by a sharp decrease in the Raman ratio from ∼ 4° to 47°. This decrease in SWNT orientation is likely caused by the volume change (∼20%) during melting and crystallization of the HDPE matrix, which is sufficient to disrupt the unidirectional SWNT orientation. The fact that both the PE crystallites and the SWNT bundles exhibit reduced but still preferred orientation after melt recrystallization indicates that the SWNT orientation dictates the PE orientation through templating PE crystal growth perpendicular to the SWNT. Thus, this system of SWNT and PE exhibits transcrystallinity.

Our findings support recent molecular dynamics simulations of carbon nanotubes and polyethylene oligomers by Wei et al.[8] that found amorphous polyethylene molecules preferentially align parallel to the nanotube axis in the melt state. This orientation in the amorphous state suggests that upon crystallization the PE crystallites will nucleate on SWNT and grow parallel to the nanotube. Li et al. describe PE crystallization in a dilute polymer solution containing SWNT or MWNT.[9] In the absence of nanotubes isolated lamellae would form, but the presence of nanotubes nucleates PE crystallites that are attached to the nanotubes. These structures resemble the shish-kebab microstructures that form when PE is crystallized in extensional flow; thus, Li et al. refer to these microstructures as "nanohybrid shish kebabs". These and our results demonstrate that SWNT indeed template the crystallization of polyethylene, in solution and in the melt, to produce transcrystalline lamellae. SWNT bundles also template the crystallization of pure sulfuric acid to form correlated crystalline orientations in a system involving stronger intermolecular forces, namely H-bonding between protonated SWNT and sulfuric acid.[29,30]

The morphological evidence for SWNT bundles templating PE crystallization with crystal growth perpendicular to these highly anisotropic objects is consistent with the thermal analysis data presented above. The Avrami exponent ($n = 1.6$) in SWNT−HDPE composites corresponds to disklike crystal growth, which is consistent with radial growth from a SWNT bundle.

Conclusions

Our new hot-coagulation method effectively fabricates SWNT−polyethylene composites and enables high SWNT loadings with good distribution. The hot-coagulation method can be applied to any amorphous or semicrystalline thermoplastic that becomes immiscible upon cooling.

SWNT nucleate PE crystal growth and accelerate the crystallization rate. Furthermore, the nanotube nucleation induces a change from three- to two-dimensional crystal growth as indicated by the change of the Avrami exponent. The addition of 1 wt % SWNT is sufficient to increase the nucleation site density such that melt fiber spinning produces shish-kebab morphologies with straight lamellae under processing conditions that otherwise produce twisted lamellae in HPDE.

SWNT bundles template PE crystallization such that lamellae grow perpendicular from the SWNT surface with the PE chains (*c*-axis) parallel to the SWNT axis. Thus, the SWNT orientation dictates the PE orientation as demonstrated in hot-pressed samples with only slight SWNT orientation, recrystallized SWNT−HDPE fibers with modest SWNT orientation, and melt-fiber-spun SWNT−HDPE fibers with nearly perfect SWNT alignment. In fact, the PE orientation factor (f_c) is higher in composite fibers than in pristine PE fibers, illustrating that templating on SWNT is more effective than extensional flow as a method for producing aligned PE morphologies.

These insights to PE nucleation and templating on SWNT provide new possibilities for engineering the interfaces within SWNT−PE nanocomposites for mechanical properties and thermal conductivity, as will be explored in future publications.

Acknowledgment. Funding for this research was provided by the National Science Foundation (DMR-MRSEC 05-20020) and the Office of Naval Research (N00014-03-1-0890 and DURINT N00014-00-1-0720).

References and Notes

(1) Bhattacharyya, A. R.; Sreekumar, T. V.; Liu, T.; Kumar, S.; Ericson, L. M.; Hauge, R. H.; Smalley, R. E. *Polymer* **2003**, *44*, 2373−2377.
(2) Grady, B. P.; Pompeo, F.; Shambaugh, R. L.; Resasco, D. E. *J. Phys. Chem. B* **2002**, *106*, 5852.
(3) Probst, O.; Moore, E. M.; Resasco, D. E.; Grady, B. P. *Polymer* **2004**, *45*, 4437.
(4) Valentini, L.; Biagiotti, J.; Kenny, J. M.; Santucci, S. *J. Appl. Polym. Sci.* **2003**, *87*, 708.
(5) Stern, T.; Wachtel, E.; Marom, G. *J. Polym. Sci., Part B: Polym. Phys.* **1997**, *35*, 2429.
(6) Assouline, A.; Wachtel, E.; Grigull, S.; Lustiger, A.; Wagner, H. D.; Marom, G. *Polymer* **2001**, *42*, 6231.
(7) Bogoeva-Gaceva, G.; Janevski, A.; Mader, E. *Polymer* **2001**, *42*, 4409.
(8) Wei, C.; Srivastava, D. *Nano Lett.* **2004**, *4*, 1949.
(9) Li, C. Y.; Li, L.; Cai, W.; Kodjie, S. L.; Tenneti, K. K. *Adv. Mater.* **2005**, *17*, 1198.
(10) Du, F.; Fischer, J. E.; Winey, K. I. *J. Polym. Sci., Part B: Polym. Phys.* **2003**, *41*, 3333.
(11) Islam, M. F.; Rojas, E.; Bergey, D. M.; Johnson, A. T.; Yodh, A. G. *Nano Lett.* **2003**, *3*, 269.
(12) Zhou, W.; Vavro, J.; Guthy, C.; Winey, K. I.; Fischer, J. E.; Ericson, L. M.; Ramesh, S.; Saini, R.; Davis, V. A.; Kittrell, C.; Pasquali, M.; Hauge, R. H.; Smalley, R. E. *J. Appl. Phys.* **2004**, *95*, 649.
(13) Fischer, J. E.; Zhou, W.; Vavro, J.; Llaguno, M. C.; Guthy, C.; Haggenmueller, R.; Casavant, M. J.; Walters, D. E.; Smalley, R. E. *J. Appl. Phys.* **2003**, *93*, 2157.
(14) Hwang, J.; Gommans, H. H.; Ugawa, A.; Tashiro, H.; Haggenmueller, R.; Winey, K. I.; Fischer, J. E.; Tanner, D. B.; Rinzler, A. G. *Phys. Rev. B* **2000**, *62*, R13310.
(15) Haggenmueller, R.; Zhou, W.; Fischer, J. E.; Winey, K. I. *J. Nanosci. Nanotechnol.* **2003**, *3*, 105.
(16) Foygel, M.; Morris, R. D.; Anez, D.; French, S.; Sobolev, V. L. *Phys. Rev. B* **2005**, *71*, 104201.
(17) Nan, C. W.; Liu, G.; Lin, Y.; Li, M. *Appl. Phys. Lett.* **2004**, *85*, 3549.
(18) Guthy, C.; Du, F.; Brand, S.; Fischer, J. E.; Winey, K. I. *MRS Proc. Fall Meeting* **2004**, *Symposium HH.*
(19) Gao, J.; Itkis, M. E.; Yu, A.; Bekyarova, E.; Zhao, B.; Haddon, R. C. *J. Am. Chem. Soc.* **2005**, *127*, 3847.
(20) Haggenmueller, R.; Fischer, J. E.; Winey, K. I. *Polymer*, in press.
(21) Huxtable, S. T.; Cahill, D. G.; Shenogin, S.; Xue, L.; Ozisik, R.; Barone, P.; Usrey, M.; Strano, M. S.; Siddons, G.; Shim, M.; Keblinski, P. *Nat. Mater.* **2003**, *2*, 731.
(22) Schultz, J. M. *Polymer Crystallization*: *The Development of Crystalline Order in Thermoplastic Polymers*; Oxford University Press: New York, 2001.
(23) Haggenmueller, R.; Gommans, H. H.; Rinzler, A. G.; Fischer, J. E.; Winey, K. I. *Chem. Phys. Lett.* **2000**, *330*, 219.
(24) Keller, A.; Machin, M. J. *J. Macromol. Sci., Phys.* **1967**, *B1*, 41.
(25) Nadkarni, V. M.; Schultz, J. M. *J. Polym. Sci., Polym. Phys. Ed.* **1977**, *15*, 2151.
(26) Dees, J. R.; Spruiell, J. E. *J. Appl. Polym. Sci.* **1974**, *18*, 1053.
(27) Hermans, J. J.; Hermans, P. H.; Vermaas, D.; Weidinger, A. *Pays-Bas* **1946**, *65*, 427.
(28) Wilchinsky, Z. W. *J. Appl. Phys.* **1960**, *31*, 1969.
(29) Zhou, W.; Fischer, J. E.; Heiney, P. A.; Fan, H.; Davis, V. A.; Pasquali, M.; Smalley, R. E. *Phys. Rev. B* **2005**, *72*, 045440.
(30) Zhou, W.; Heiney, P. A.; Fan, H.; Smalley, R. E.; Fischer, J. E. *J. Am. Chem. Soc.* **2005**, *127*, 1640.

MA0527698